



# Analytical modeling of cutting forces considering material softening effect in laser-assisted milling of AerMet100 steel

Hang Zhang<sup>1</sup> · Haohao Zeng<sup>2</sup> · Rong Yan<sup>1</sup> · Wei Wang<sup>1</sup> · Fangyu Peng<sup>3</sup>

Received: 15 August 2020 / Accepted: 15 December 2020 / Published online: 23 January 2021  
© The Author(s), under exclusive licence to Springer-Verlag London Ltd. part of Springer Nature 2021

## Abstract

AerMet100 steel is a typical difficult-to-cut material, and laser-assisted milling (LAM) is a promising machining technology for this kind of material. In LAM process, the material is softened by the thermal effect of laser beam, which improves the machinability of the materials. And finally, the cutting forces are reduced compared with conventional milling (CM). This paper presents an analytical model considering material softening effect to predict the cutting force during LAM. The cutting force is produced by shearing and ploughing action. Both laser source and cutting tool are discretized into elements. Based on the Johnson-Cook (J-C) constitutive model and the thermal model due to laser beam and cutting action, the shear plane temperature and the shear flow stress considering the combined effects of laser heating and plastic deformation are calculated iteratively, and the influence of material softening effect on cutting force coefficients is taken into account. A series of experiments carried out on AerMet100 steel demonstrate the accuracy of the cutting force model, and the results show that the three-axis cutting force in LAM is reduced by up to 33.9%. Besides, the influence of laser parameters related to material softening effect on the cutting force is discussed based on the proposed model.

**Keywords** Laser-assisted milling (LAM) · AerMet100 steel · Cutting forces · Material softening effect · Shear flow stress

## 1 Introduction

Ultrahigh strength steel AerMet100, with excellent comprehensive mechanical properties, is an advanced material for manufacturing important structural parts such as carrier aircraft landing gear. However, AerMet100 steel is also a typical difficult-to-cut material and its poor machinability will result in surface damage and low tool life during CM process. In

order to overcome the difficulties in machining difficult-to-cut materials, some compound processing technologies have been developed. Among them, laser-assisted milling (LAM) is a promising technology applied in machining difficult-to-cut materials. In the research of laser material processing technology (such as laser welding [1, 2]), the effect mechanism of laser on materials is very complex, and naturally, it is more difficult to reveal the processing mechanism under the combined action of laser heating and cutting. During LAM, the material is softened by the thermal effect of laser beam, which causes a reduction in cutting forces and improves the machinability of the material compared with CM. Research on LAM is a hot topic at present.

Many studies have shown that LAM performs well in machining difficult-to-cut materials. Hu et al. [3] combined laser heating with grinding to machine difficult-to-cut materials. The experimental results indicated that the surface roughness of workpiece was smaller and the hardness distribution of surface was more uniform after laser-assisted machining. Kim and Lee [4] conducted laser-assisted machining experiments on AISI 1045, Inconel 718, and titanium alloy respectively. Their research proved that laser-assisted machining technology can improve the surface quality of workpiece. In

---

✉ Rong Yan  
yanrong@hust.edu.cn

Hang Zhang  
zh5101@hust.edu.cn

<sup>1</sup> National NC System Engineering Research Center, School of Mechanical Science and Engineering, Huazhong University of Science and Technology, Wuhan 430074, China

<sup>2</sup> Nanjing Research Institute of Electronics Technology, Nanjing 210039, China

<sup>3</sup> State Key Lab of Digital Manufacturing Equipment and Technology, School of Mechanical Science and Engineering, Huazhong University of Science and Technology, Wuhan 430074, China

addition, compared with conventional machining, laser-assisted machining can also reduce specific machining energy [5], increase material removal rate [6], suppress chatter [7], and extend tool life [8].

In the traditional machining process, the main means to study the machining mechanism are experimental [9], finite element (FE) [10], and analytical methods [11]. Mastering the machining mechanism of LAM is the prerequisite for the successful application of this technology. In order to reveal the machining mechanism of LAM, an accurate cutting force model must be established. During laser-assisted machining, the cutting forces are significantly affected by the softening behavior of materials caused by laser heating. Many researchers have studied cutting forces in thermally enhanced machining by using FE simulation and empirical and analytical methods respectively.

Özel and Pfefferkorn [12] presented a FE model of laser-assisted micro-milling to explore the effect of laser heating on cutting forces. The laser preheating temperature in the uncut chip zone was approximated as a fixed value and used as the initial condition of the FE simulation. Xi et al. [13] presented a FE model of thermally enhanced machining on Ti6Al4V. The simulation results under different initial temperature conditions indicated that the root cause for the reduction in cutting forces was the decrease of shear flow stress caused by the increase in shear plane temperature. Pan et al. [14] also presented a FE model to predict cutting forces in LAM of Incon718 based on DEFORM software. The motion of laser spot was simulated by defining time-dependent temperature boundary conditions.

Kim and Lee [15] established an empirical model of cutting forces in LAM of different materials (Inconel 718 and AISI 1045 steel) by using statistical regression analysis. The main cutting force was expressed as a quadratic polynomial of spindle speed, feed speed, and cutting depth with fixed tool diameter and laser power. Woo and Lee [16] used a similar method to predict cutting forces in LAM of Ti6Al4V and Inconel 718 alloy respectively.

Singh and Melkote [17] developed an analytical model to predict cutting forces in laser-assisted micro-grooving based on the slip-line field theory. In the model, the temperature rise due to laser heating was taken as shear plane temperature, and shear flow stress was calculated by the material flow stress equation. Kumar et al. [18] proposed an iterative algorithm for calculating shear plane temperature considering the combined effects of laser heating and plastic deformation to predict cutting forces in laser-assisted micro-milling. The average temperature in the axial depth of cut region after laser heating was used as the initial value of the algorithm, and the yield strength of the material corresponding to the shear plane temperature was approximated to the shear flow stress. Elhami et al. [19] studied the combination of external concentrated heat source and ultrasonic vibrations in milling process. An analytical

model was developed based on consideration of thermal softening of material caused by the concentrated heat source to predict cutting forces during the hybrid milling process. The temperature at the theoretical tip point after laser heating was taken as the shear plane temperature, and then, the shear flow stress and cutting forces were calculated in turn. In order to predict cutting forces in LAM, Pan et al. [20] established an analytical model, which considered the effect of the dynamic recrystallization effect of material on shear flow stress, and took the temperature after laser preheating as the ambient temperature.

The analytical model based on theory can characterize the influence of each parameter on cutting forces, so as to better elaborate the machining mechanism. As for analytical models, most researchers only considered temperature rise due to laser heating and ignored the influence of plastic deformation during the cutting process to calculate the shear plane temperature. Although other researchers have calculated the shear plane temperature under the combined effects of laser heating and plastic deformation, the shear flow stress has not been solved clearly.

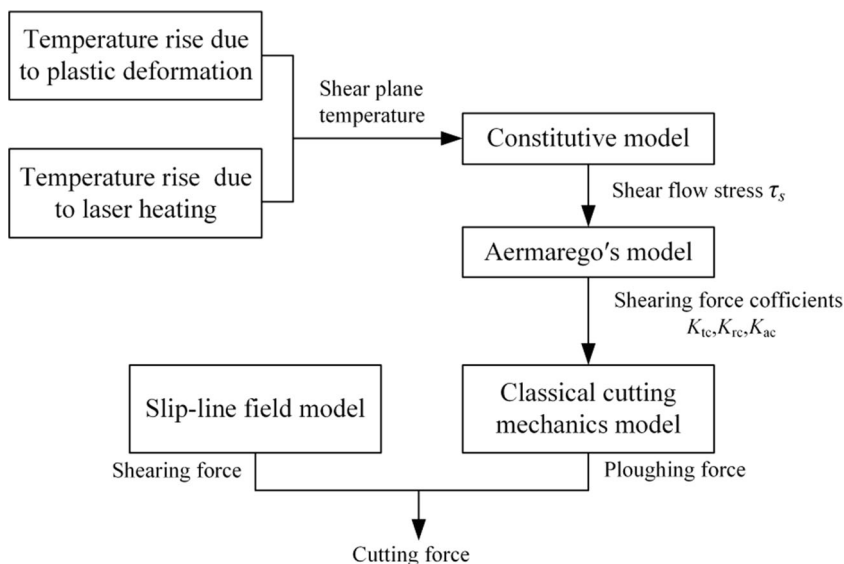
The main purpose of this paper is to establish an accurate analytical model, which is capable of predicting the cutting force during LAM process. Based on the heat conduction theory, the unequal division shear zone model, and the J-C constitutive model, shear plane temperature and shear flow stress considering the combined effects of laser heating and plastic deformation are calculated iteratively. Meanwhile, ploughing force is taken into account as well.

In Section 2, the modeling procedure of the cutting force considering shearing and ploughing is elaborated. Shear plane temperature and shear flow stress considering material softening effect during LAM are calculated in Section 3. Section 4 introduces model verification and discussion. Conclusions of the entire study are summarized in Section 5.

## 2 The cutting force model for LAM

Cutting force is considered not only an important index for evaluating the feasibility of LAM technology but also the basis for exploring the machining mechanism. In this paper, an analytical model based on theory is proposed to predict the cutting force in LAM. The overall flow of cutting force prediction is shown in Fig. 1. Based on the slip-line field theory and classical cutting mechanics theory, the three-axis cutting force ( $F_x$ ,  $F_y$ ,  $F_z$ ) is obtained. In order to simulate the actual working condition of LAM, the influence of shear flow stress under the combined action of laser heating and plastic deformation on each cutting force coefficient is taken into account. The shear flow stress is calculated iteratively by combining the temperature rise model considering laser heating and

**Fig. 1** Overall flow of cutting force prediction



plastic deformation and constitutive model, and the detailed process will be described in Section 3.

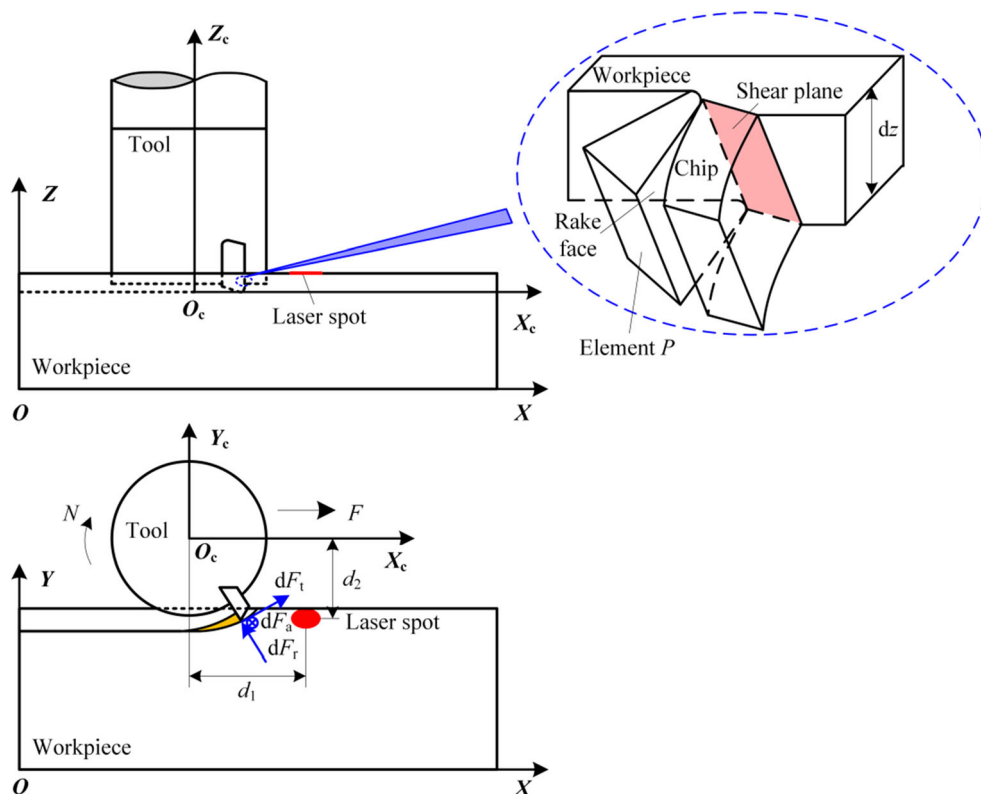
**2.1 Elemental cutting force**

A square shoulder milling cutter with one insert is used and the milling mode is down-milling in this study. The milling tool is discretized into elements at equal intervals  $dz$  along the tool axis to tackle the problems of interrupted cutting process

and complex cutter geometry. The motion of each element can be considered as an independently oblique cutting process.

Figure 2 shows the schematic diagram of LAM process. Tool coordinate system  $O_c X_c Y_c Z_c$  is established in Fig. 2; it moves together with the cutter at the same feed speed  $F$  along the direction of  $O_c X_c$ . And the relative position of the tool and the laser heat source are determined by  $d_1$  and  $d_2$ , where  $d_1$  and  $d_2$  represent the distance between laser spot center and tool center in the  $X$  and  $Y$  directions respectively. An arbitrary

**Fig. 2** LAM process schematic



element  $P$  at elevation  $z$  is taken as an example to illustrate the geometrical relationship between tool and workpiece.

Radial immersion angle  $\varphi(z)$  and axial immersion angle  $\kappa(z)$  of the arbitrary element  $P$  in Fig. 2 can be formulated as follows:

$$\varphi(z) = \varphi_0 - \frac{2z}{D} \tan\beta \tag{1}$$

$$\kappa(z) = \begin{cases} \cos^{-1}\left(\frac{r_0-z}{r_0}\right) & z \leq r_0 \\ \pi/2 & z > r_0 \end{cases} \tag{2}$$

where  $\varphi_0$  is defined as the radial immersion angle of the insert at elevation zero.  $\beta$ ,  $D$ , and  $r_0$  are the helix angle, diameter, and corner radius of the cutter respectively.

The cutting force is calculated on the premise that the cutting edge meshes with the workpiece. The meshing state is judged by comparing elemental radial immersion angle with the angles of cutting entry and exit. In the down-milling process, the angles of cutting entry and exit can be formulated as follows:

$$\begin{cases} \varphi_{st}(z) = \pi/2 + \sin^{-1}\left(\frac{D/2-a_e}{R(z)}\right) \\ \varphi_{ex}(z) = \pi \end{cases} \tag{3}$$

where  $a_e$  and  $R(z)$  are the radial depth of cut and the effective cutting radius of element  $P$  respectively.

Shearing force and ploughing force should be calculated to evaluate cutting force, when the tool is not absolutely sharp. Elemental tangential ( $dF_t$ ), radial ( $dF_r$ ), and axial ( $dF_a$ ) cutting forces acting on element  $P$  can be determined as follows [21]:

$$\begin{cases} dF_t(z) = K_{tc}h_a(z)db + dF_{tp} \\ dF_r(z) = K_{rc}h_a(z)db + dF_{rp} \\ dF_a(z) = K_{ac}h_a(z)db + dF_{ap} \end{cases} \tag{4}$$

where  $K_{tc}$ ,  $K_{rc}$ , and  $K_{ac}$  are the shearing force coefficients in tangential, radial, and axial directions respectively, and these coefficients will be obtained in Section 2.2.  $dF_{tp}$ ,  $dF_{rp}$ , and  $dF_{ap}$  are elemental tangential, radial, and axial ploughing forces respectively, and they can be determined from the slip-line field model proposed by Waldorf et al. [22].  $db$  is the projected length of element  $P$  in the direction of cutting velocity.  $h_a = f_z \cdot \sin\varphi \cdot \sin\kappa$ ,  $db = dz/\sin\kappa$ ,  $f_z$  is the feed rate, and  $\varphi$  and  $\kappa$  are the radial and axial immersion angles of element  $P$  respectively.

Three orthogonal cutting force components of element  $P$  in workpiece coordinate system  $OXYZ$  can be derived from elemental tangential, radial, and axial cutting forces by the following coordinate transformation:

$$\begin{bmatrix} dF_x(\tau, z) \\ dF_y(\tau, z) \\ dF_z(\tau, z) \end{bmatrix} = \begin{bmatrix} -\cos\varphi & -\sin\varphi\sin\kappa & -\sin\varphi\cos\kappa \\ \sin\varphi & -\cos\varphi\sin\kappa & -\cos\varphi\cos\kappa \\ 0 & \cos\kappa & -\sin\kappa \end{bmatrix} \begin{bmatrix} dF_t(\tau, z) \\ dF_r(\tau, z) \\ dF_a(\tau, z) \end{bmatrix} \tag{5}$$

Furthermore, three orthogonal components of the total instantaneous cutting force with cutting depth  $a_p$  on the cutting tool caused by all elements can be determined as the following expression:

$$\begin{cases} F_x(\tau) = \int_0^{a_p} dF_x(\tau, z) \\ F_y(\tau) = \int_0^{a_p} dF_y(\tau, z) \\ F_z(\tau) = \int_0^{a_p} dF_z(\tau, z) \end{cases} \tag{6}$$

### 2.2 Calculation of shearing force coefficients

According to the oblique cutting model proposed by Armarego and Brown [23], shearing coefficients can be estimated by Eq. (7).

$$\begin{cases} K_{tc} = \frac{\tau_s}{\sin\phi_n} \frac{\cos(\beta_a - \alpha_n) + \tan i_n \tan \eta_c \sin\beta_a}{\sqrt{(\cos(\phi_n + \beta_a - \alpha_n))^2 + (\tan \eta_c \sin\beta_a)^2}} \\ K_{rc} = \frac{\tau_s}{\sin\phi_n \cos i_n} \frac{\sin(\beta_a - \alpha_n)}{\sqrt{(\cos(\phi_n + \beta_a - \alpha_n))^2 + (\tan \eta_c \sin\beta_a)^2}} \\ K_{ac} = \frac{\tau_s}{\sin\phi_n} \frac{\cos(\beta_a - \alpha_n) \tan i_n - \tan \eta_c \sin\beta_a}{\sqrt{(\cos(\phi_n + \beta_a - \alpha_n))^2 + (\tan \eta_c \sin\beta_a)^2}} \end{cases} \tag{7}$$

where  $\tau_s$  is the shear flow stress.  $\beta_a$ ,  $\alpha_n$ , and  $\phi_n$  are the normal friction, and rake and shear angles respectively. The angle of inclination  $i_n$  of the helical cutting edge to the cutting velocity is equal to the cutter's helix angle  $\beta$ .  $\eta_c$  is the chip flow angle which approximately equals to the inclination angle  $i_n$  [24].

Shear flow stress  $\tau_s$  is proportional to the shearing force coefficients and is the key to the calculation of cutting force. In LAM,  $\tau_s$  is comprehensively affected by laser heating and plastic deformation, and the solving process of  $\tau_s$  will be introduced in Section 3.

In the process of machining, when uncut chip thickness is close to or less than the cutting edge radius, an effective rake angle plays a more important role than a nominal rake angle. Therefore, the normal rake angle  $\alpha_n$  is replaced by the effective rake angle  $\alpha_e$  in the process of calculating cutting force. The effective rake angle model [25] is used to calculate the elemental effective rake angle, as shown in the following formula:

$$\alpha_e = \begin{cases} \tan^{-1} \left[ \frac{-\sqrt{(2-\zeta h_a/r_e)\zeta h_a/r_e} - \sin\theta_f}{\zeta h_a/r_e - 1 + \cos\theta_f} \right] & h_a/r_e \leq 1 + \sin\alpha_0 \\ \tan^{-1} \left[ \frac{(\zeta h_a/r_e - 1)\tan\alpha_0 - \sec\alpha_0 + \sin\theta_f}{\zeta h_a/r_e - 1 + \cos\theta_f} \right] & h_a/r_e > 1 + \sin\alpha_0 \end{cases} \tag{8}$$

where  $r_e$  and  $\alpha_0$  are the cutting edge radius and nominal rake angle respectively. Empirical constant  $\zeta$  is taken as 2 [26].  $\theta_f$  is the separation angle between tool and chip, which is taken as  $37.6^\circ$  [27].

According to Ref. [28], the normal friction angle  $\beta_a$  can be determined from the following relation:

$$\begin{cases} \tan\beta_a = \frac{\tau_1}{P_0} \left\{ 1 + \xi \left[ 1 - \left( \frac{\tau_1}{\mu P_0} \right)^{1/\xi} \right] \right\} \\ \frac{\tau_1}{P_0} = \frac{\xi + 2}{4(\xi + 1)} \frac{\sin[2(\phi_n + \beta_a - \alpha_n)]}{(\cos\beta_a)^2} \end{cases} \quad (9)$$

where  $\mu$  is the sliding friction coefficient between rake face and workpiece; it is solved inversely by the particle swarm optimization (PSO) algorithm based on the predicted and measured data of CM and equal to 0.78.  $\tau_1$  is the shear yield stress of the bonded zone on rake face.  $P_1$  is the normal pressure at the tool tip on the rake face. Empirical constant  $\xi$  is considered as 3.

The normal shear angle  $\phi_n$  can be calculated by the shear angle model proposed by Merchant [29]:

$$\phi_n = \frac{\pi}{4} + \frac{\alpha_n}{2} - \frac{\beta_a}{2} \quad (10)$$

### 3 Shear flow stress considering material softening effect

The solution of shear flow stress is the key to calculating cutting forces. In LAM process, the material is softened by laser heating before shear action, which results in a significant rise in the temperature of the shear zone. In analytical models of cutting forces in LAM proposed by predecessors, some

$$T_{sl}(z) = \sum_{i=1}^{N_1} \sum_{j=1}^{N_2} \left\{ \frac{a_0 P_{dij} S_{ij}}{2\pi\tau\lambda} \left[ \frac{1}{s_{ij}} \exp\left(-F \frac{s_{ij} + x_0 - x_{ij}}{2\alpha}\right) + \frac{1}{s_{ij}^1} \exp\left(-F \frac{s_{ij}^1 + x_0 - x_{ij}}{2\alpha}\right) \right] \right\} + T_r \quad (11)$$

where  $N_1$  and  $N_2$  are the angular and radial discrete numbers of the laser heat source respectively, and the range of variables  $i$  and  $j$  is determined by  $N_1$  and  $N_2$ .  $a_0$  is the absorptivity of AerMet100 steel in the laser. Through calibration experiments, the empirical formula of absorptivity is  $a_0 = 0.5652P_0^{-0.1536} F^{0.0793}$ , where  $P_0$  is the laser power.  $P_{dij}$  and  $S_{ij}$  are the power density and area of the  $ij$ th point heat source  $N_{ij}$  respectively.  $\alpha$  and  $\lambda$  are the thermal diffusivity and thermal conductivity of the workpiece material.  $s_{ij}$  and  $s_{ij}^1$  are the distances from the cutting edge element to  $N_{ij}$  and image point heat source  $N_{ij}^1$  respectively.  $x_0$  and  $x_{ij}$  are the  $x$ -coordinates of the cutting edge element and the point heat source  $N_{ij}$  respectively, and the distance between  $x_0$  and  $x_{ij}$  increases with the increase of laser-tool distance  $d_1$ .  $T_r$  is the ambient temperature.

During LAM, the distance between different cutting edge elements and the laser spot is different, so the corresponding

researchers took the temperature of the shear plane caused by laser heating as the shear plane temperature, while others adopted approximation of shear flow stress. In this section, the effect of laser heating on the plastic deformation of shear zone is considered, and an accurate method for calculating the shear plane temperature and shear flow stress under the combined action of laser heating and plastic deformation is presented.

### 3.1 Calculation of shear flow stress

#### 3.1.1 Preheating temperature of shear plane

The calculation of preheating temperature of shear plane is the basis of calculating shear plane temperature. According to Ref. [30], a temperature model of laser heating process is built to predict the preheating temperature distribution of workpiece. The laser heat source is discretized into point heat sources in both angular and radial directions to calculate the temperature of any point  $M(x, y, z)$  on the workpiece. The angular and radial positions of the point heat sources are determined by the variables  $i$  and  $j$ . The image heat sources of the laser heat source are added to satisfy the adiabatic boundary of workpiece [31]. Taking an arbitrary point heat source  $N_{ij}$  as an example, the schematic diagram of laser temperature model is shown in Fig. 3.

When point  $M$  is the cutting edge tip point, the temperature at point  $M$  is the preheating temperature of the shear plane. Therefore, the preheating temperature  $T_{s1}$  of the shear plane in LAM process corresponding to each cutting edge element can be obtained by Eq. (11).

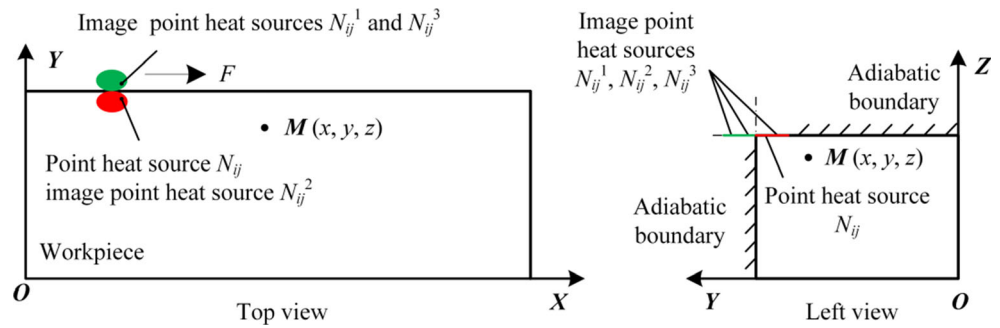
preheating temperature of the shear plane is not the same. For the same element, the relative position of the element and laser spot changes due to the rotation of tool, so there is also a difference in the preheating temperature of the corresponding shear plane.

#### 3.1.2 Shear plane temperature and shear flow stress

The J-C constitutive model is used to solve the shear flow stress on the main shear plane during the cutting process of each cutting edge element:

$$\tau_s = \frac{1}{\sqrt{3}} (A + B\varepsilon^n) \left( 1 + C \ln \left( \frac{\dot{\varepsilon}}{\varepsilon_0} \right) \right) \left( 1 - \left( \frac{T_s - T_r}{T_m - T_r} \right)^m \right) \quad (12)$$

**Fig. 3** Schematic diagram of laser temperature model



where  $A, B, n, C$ , and  $m$  are the J-C constitutive parameters of the workpiece material.  $\varepsilon$  and  $\dot{\varepsilon}$  are the equivalent plastic strain and equivalent plastic strain rate respectively, which can be determined by Eq. (13). The reference plastic strain rate  $\dot{\varepsilon}_0$  is set as 1.  $T_m$  is the material melting temperature. Shear plane temperature  $T_s$  will be derived later.

$$\begin{cases} \varepsilon = \frac{c_0 \cos \alpha_n}{\sqrt{3} \cos(\phi_n - \alpha_n) \sin \phi_n} \\ \dot{\varepsilon} = \frac{2V \cos \alpha_n}{\sqrt{3} t_a \cos(\phi_n - \alpha_n)} \end{cases} \quad (13)$$

where  $c_0$  is the proportion of the main shear zone, which can be solved by Eq. (14).  $V$  is the cutting velocity of cutting edge element.  $t_a$  is the thickness of the main shear zone, which is taken to be half of the instantaneous uncut chip thickness [32].

$$c_0 = \frac{1}{2} + \frac{\cos(2\phi_n - \alpha_n)}{2 \cos \alpha_n} \quad (14)$$

According to the non-equal shear zone model proposed by Tounsi et al. [33], the main shear plane temperature  $T_s$  of the cutting edge element in LAM can be derived as follows:

$$T_s = T_0 + \frac{c_0(2\tau_s + \tau_0) \cos \alpha_n}{3\rho c \sin \phi_n \cos(\phi_n - \alpha_n)} \quad (15)$$

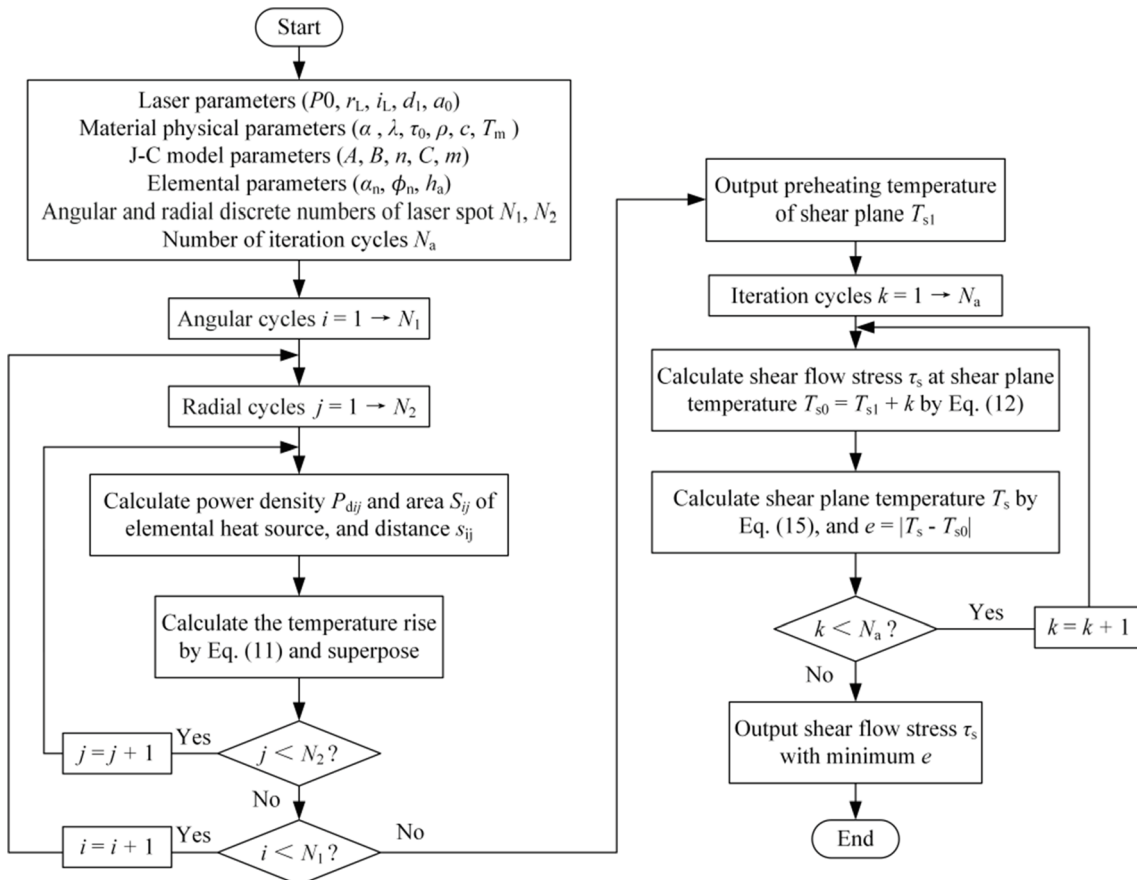


**Fig. 4** Flow chart for calculating elemental shear flow stress in LAM

**Table 1** Simulation scheme of CM

Spindle speed $N$ (r/min)	Feed rate $f_z$ (mm/tooth)	Axial depth of cut $a_p$ (mm)	Radial depth of cut $a_e$ (mm)	Tool diameter $D$ (mm)
1000	0.05	2	4	25
Corner radius $r_0$ (mm)	Edge radius $r_e$ ( $\mu\text{m}$ )	Nominal rake angle $\alpha_0$ ( $^\circ$ )	Helix angle $\beta$ ( $^\circ$ )	Milling mode
0.8	32.48	5.6	3.25	Down-milling

where  $T_0$  is the room temperature, while it is replaced by the preheating temperature  $T_{sl}$  of shear plane in LAM.  $\tau_0$ ,  $\rho$ , and  $c$  are shear stress at main shear zone inlet, mass density, and specific heat of workpiece material respectively.

The shear flow stress  $\tau_s$  on the main shear plane of the cutting edge element in Section 2.2 can be determined by combining Eqs. (12) and (15). The flow chart for calculating elemental shear flow stress in LAM is outlined in Fig. 4.

### 3.2 Comparison of models

At present, in most research on cutting forces during LAM process, only the temperature rise due to laser heating was considered, while the heat produced by plastic deformation during cutting was ignored, such as the model proposed by Elhami et al. [19]. The shear plane temperature and shear flow stress under CM, LAM, and Elhami model respectively were compared by the analytical model proposed in this paper to reveal the softening behavior of materials caused by laser heating in LAM. Among them, the simulation scheme of CM is shown in Table 1. For LAM, the parameters are identical to CM except for laser power. The shear plane temperature of the Elhami model is the laser preheating temperature, and the temperature rise due to plastic deformation is not considered. In addition, laser power  $P_0$  is 500 W, radius of laser beam  $r_L$  is 1.8 mm, laser incidence angle  $i_L$  is  $45^\circ$ , and laser-tool distance  $d_1$  is 13 mm.

The simulation results of shear plane temperature and shear flow stress under three different conditions are shown in Fig. 5. Figure 5a shows the shear plane temperature. In CM, the shear plane temperature increases with the increase of rotation angle of tool. This is because the instantaneous uncut chip thickness decreases gradually with the increase of radial

immersion angle in down-milling mode, which leads to the phenomenon of cutting with negative rake angle more and more obvious. The shear plane temperature in LAM is higher than that in CM under the influence of laser heating. In the Elhami model, the shear plane temperature decreases gradually as the milling process progresses. This is attributed to the fact that the laser heat source is gradually far away from the cutting edge element and the effect of plastic deformation on temperature is neglected.

As shown in Fig. 5b, the change trend of shear flow stress is completely opposite to that of shear plane temperature. Furthermore, shear flow stress in LAM is less than that in CM, and the values of both tend to be equal as the tool rotates. This phenomenon indicates that there is a softening effect of materials in LAM and the softening effect decreases with the progress of cutting. This is because the distance between the cutting edge element and laser spot becomes longer during the process of cutting entry and exit, which causes the decrease of shear plane temperature. While in the Elhami model which only considered the laser heating temperature, shear flow stress increases with the decrease of the shear plane temperature and is even higher than that in CM.

Therefore, compared with the Elhami model, the model established in this paper reflects the material flow behavior under the combined action of laser heating and plastic deformation more objectively. Compared with CM, a significant material softening effect is observed in LAM.

### 4 Model verification and discussion

In order to validate the cutting force model, LAM experiments were carried out in this part. The three-axis cutting force ( $F_x$ ,

**Fig. 5** Comparison of CM, LAM, and Elhami model. **a** Shear plane temperature. **b** Shear flow stress

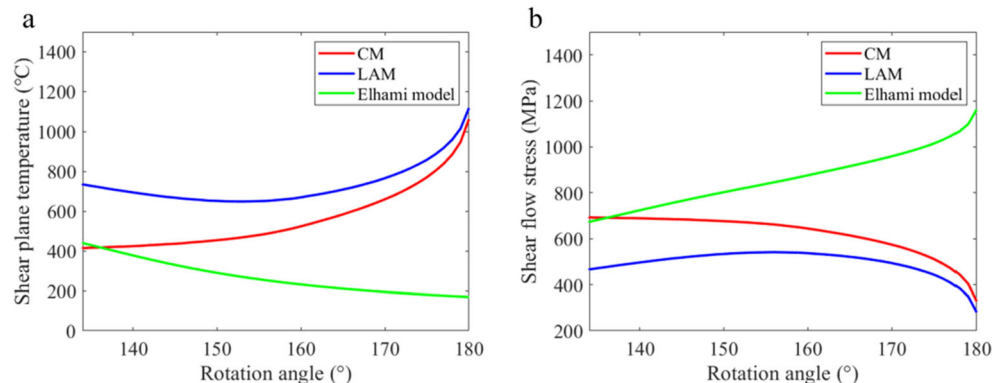


**Table 2** Chemical composition of AerMet100 steel [34]

C	Mn	Si	Ni	Cr	Mo	Al	Co	Ti	O	N	S+P	Fe
0.225	0.01	0.01	11.22	3.04	1.20	0.015	13.50	≤ 0.015	≤ 0.002	≤ 0.0015	≤ 0.01	balance

$F_y, F_z$ ) in machining was measured by a dynamometer (Kistler, 9129AA). Based on the quantitative analysis, the cutting force model presented in this paper was verified. Besides, the influences of process parameters related to material softening effect on the cutting force were theoretically investigated.

#### 4.1 LAM experiments

The workpiece is a block of AerMet100 steel with a length of 100 mm, a width of 30 mm, and a height of 30 mm, and its bulk hardness is about 38–40 HRC. The main chemical composition and material properties of AerMet100 steel used in this paper are listed in Tables 2 and 3 respectively. The J-C constitutive parameters of AerMet100 steel were calibrated by the particle swarm optimization (PSO) algorithm based on the shear flow stress obtained from orthogonal cutting experiments and J-C constitutive equations respectively. The calibration result is listed in Table 4.

All experiments were performed on the self-built LAM platform shown in Fig. 6. A diode laser generator (HDLS-1000) with the maximum output power of 1000 W was used. The collimating optic focused the laser onto the workpiece surface to realize laser heating. A fixture was designed to clamp the collimating optic and was fixed on the spindle. A square shoulder milling cutter (Kennametal, STELLRAM 7690VA12CA025Z03R40-3) with 25 mm diameter was used in this study. Only one carbide insert (Kennametal, ADHT12T308ER-46 SP6519) was installed on the cutter, and a new carbide insert was used in each experiment. The experimental scheme is shown in Table 5. In addition, spindle speed  $N$ , radial depth of cut  $a_e$ , axial depth of cut  $a_p$ , laser incident angle  $i_l$ , and laser-tool distance (in the  $X$  direction)  $d_1$  were kept invariant, and equal to 1000 r/min, 4 mm, 2 mm, 45°, and 13 mm respectively. Down-milling was chosen as the milling mode in this investigation.

**Table 3** Main material properties of AerMet100 steel

Density $\rho$ (kg/m <sup>3</sup> )	Thermal diffusivity $\alpha$ (m <sup>2</sup> /s)	Thermal conductivity $\lambda$ (W/m·°C)	Specific heat capacity $c$ (J/kg·°C)
7889	126	19.3	412.7

#### 4.2 Experimental results

The cutting force model established in this paper is used to predict the three-axis cutting force under each experimental parameter, and the cutting force of LAM is predicted by the Elhami model too. The predicted and measured three components of cutting force are shown in Fig. 7. The amplitude of cutting forces is also used as an evaluation index. The results of the comparison between the predicted and the measured amplitude of the three-axis cutting force are shown in Table 6.

Figure 7 shows that the cutting force model established in this paper is more accurate than the Elhami model in predicting the cutting force of LAM. This is because the Elhami model ignores the temperature rise generated by plastic deformation, which increases the shear flow stress (as shown in Fig. 5). Furthermore, the predicted cutting force is significantly larger. Meanwhile, as shown in Table 6, the average relative error of the maximum cutting force in the  $X$ ,  $Y$ , and  $Z$  directions is about 7.5%. Overall, the consistence between experimental and predicted results demonstrates the good prediction accuracy of the proposed cutting force model.

In addition, the effects of laser power and laser scanning speed on the cutting force during LAM are shown in Figs. 8 and 9 respectively, which include both experimental and prediction results. The graphs show that the predicted and experimental influences are consistent, which verify the effectiveness of the proposed model again.

#### 4.3 Influences of laser parameters on cutting force

When the material is softened by thermal effect, the energy required for plastic deformation during cutting process is reduced, which makes the material prone to shearing. Therefore, in LAM, the material softening effect caused by laser heating is the primary reason for the reduction of cutting forces. The strength of material softening is determined by the heat generated by laser heat source. According to the self-built experimental platform shown in Fig. 6, it is obvious that the softening degree of material is controlled by laser power, laser

**Table 4** J-C constitutive model parameters of AerMet100 steel

$A$ (MPa)	$B$ (MPa)	$n$	$C$	$m$
831.8	731.3	0.2893	0.01	0.8571



**Table 5** Experimental parameters

No.	Laser power $P_0$ (W)	Feed rate $f_z$ (mm/tooth)	No.	Laser power $P_0$ (W)	Feed rate $f_z$ (mm/tooth)
1	0	0.05	6	500	0.075
2	250	0.05	7	0	0.1
3	500	0.05	8	250	0.1
4	0	0.075	9	500	0.1
5	250	0.075	10	750	0.1

scanning speed, and laser-tool distance (in the  $X$  direction). In this section, AerMet100 steel and the amplitude of the three-axis cutting force are used as the research material and the evaluation index respectively. The influence of laser parameters that can control the strength of the material softening effect on the cutting force of LAM is discussed.

#### 4.3.1 Laser power

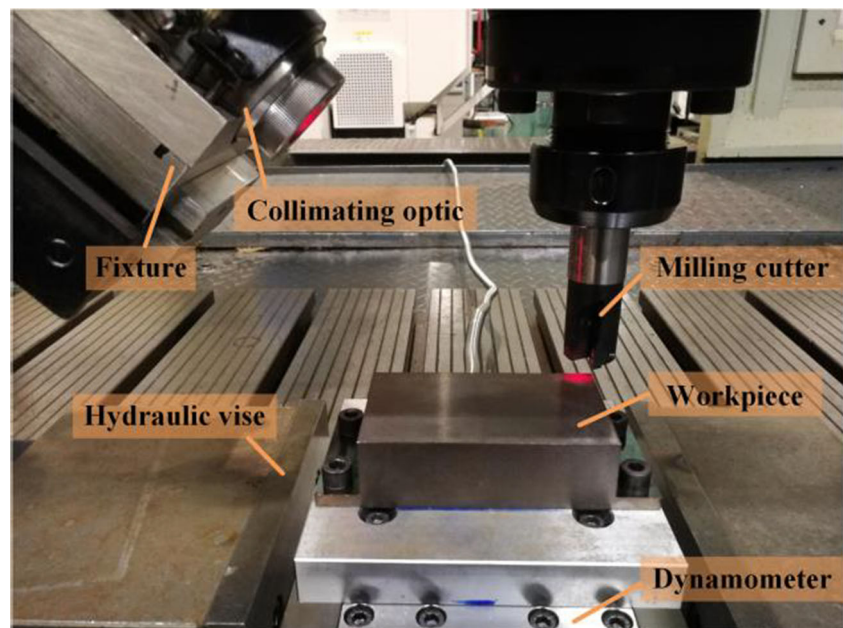
The effect of laser power on the three-axis cutting force of LAM is shown in Fig. 8. Obviously, the amplitude of cutting forces decreases with the increase of laser power, even if the machining is carried out with different feed rate. The reason is that the increase of laser power intensifies the softening degree of the material, which leads to the increase of shear plane temperature and the decrease of shear flow stress. Taking experiment Nos. 7–10 as an example, the cutting force can be reduced by up to 40% in LAM, compared with CM.

Theoretically, the larger the laser power is, the higher the material softening degree will be, and the smaller the cutting force will be. However, excessive laser power will cause the residual heat affected zone. From the work in Ref. [25], the experimental parameters in Table 5 of each group all meet the

requirements of yielding no residual heat affected zone in the machined surface layer. Therefore, LAM processing of AerMet100 steel can reduce the cutting force under appropriate process parameters.

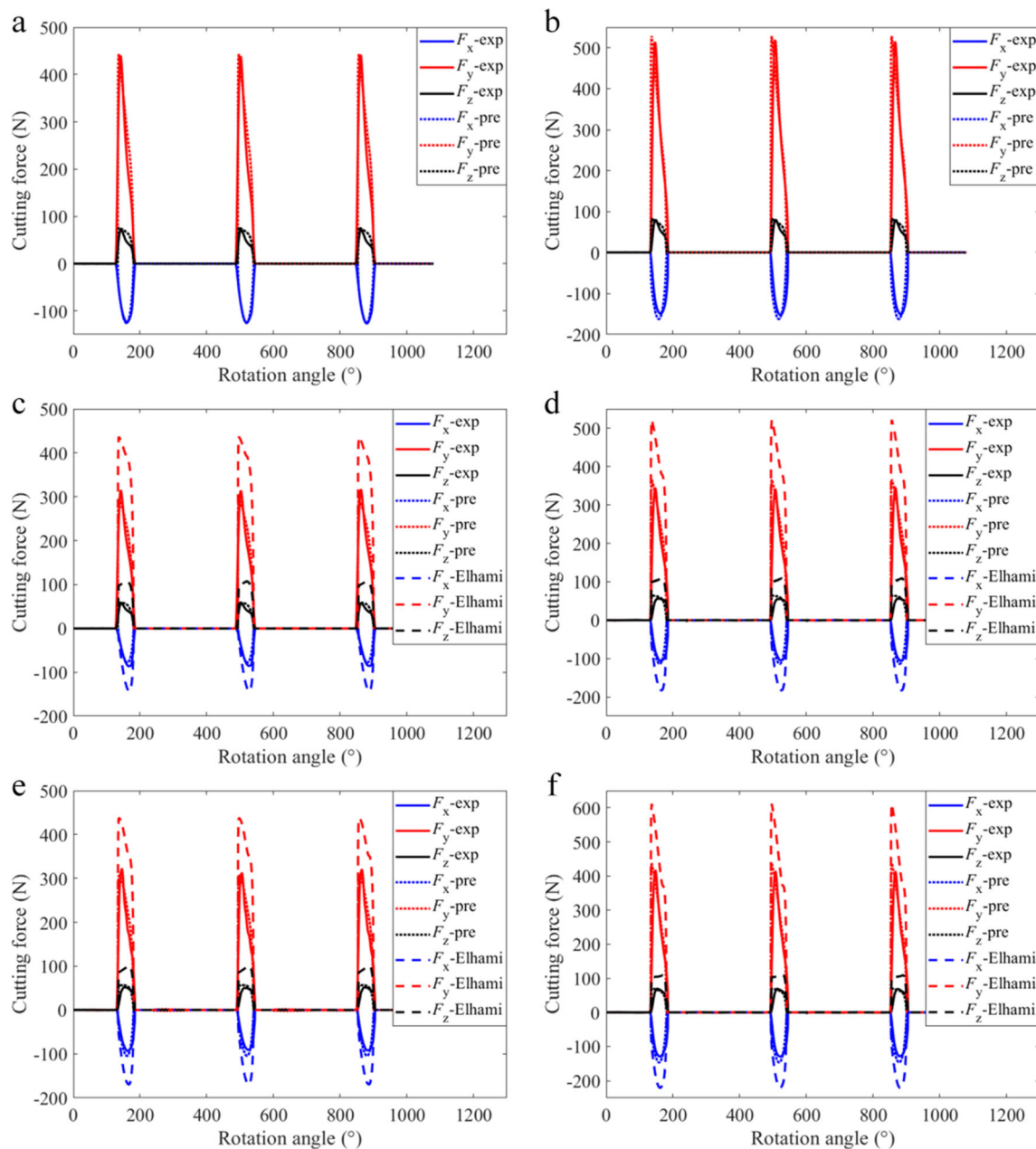
#### 4.3.2 Laser scanning speed

In the LAM experimental platform shown in Fig. 6, the laser device was fixed on the machine spindle and moved synchronously with it. When the spindle speed is constant, the laser scanning speed is adjusted by changing the feed rate. Figure 9 shows the effect of laser scanning speed on the amplitude of the three-axis cutting force when machining with different laser powers. It can be seen from the figure that the amplitude of the cutting force increases obviously with the increase of laser scanning speed. There are two reasons. One is that the increase of laser scanning speed shortens the heating time of the material, which reduces the preheating temperature of shear plane and the degree of material softening. The other is that the increase of laser scanning speed also represents the increase of feed rate, which results in a proportional increase in the instantaneous uncut chip thickness. Moreover, it can be found that the cutting force components  $F_x$  and  $F_z$  are the most

**Fig. 6** LAM experimental platform

**Table 6** Verification test results

No.	$F_{x(amp)}$			$F_{y(amp)}$			$F_{z(amp)}$		
	Exp (N)	Pre (N)	Error (%)	Exp (N)	Pre (N)	Error (%)	Exp (N)	Pre (N)	Error (%)
1	101.4	85.6	15.6	343	357.1	4.1	70	69.7	0.4
2	85.8	77.8	9.3	314.6	294.9	6.3	57.6	58.9	2.3
3	76.2	71.8	5.8	265.1	247.4	6.7	46.7	52.2	11.8
4	125.5	125.6	0.08	439.6	443.5	0.9	71.2	76.2	7.0
5	105.4	113.9	8.1	343.2	366.4	6.8	56	64.6	15.4
6	92.4	104.8	13.4	318.1	306.8	3.6	51.4	56.7	10.3
7	150.4	162.3	7.9	515.4	528.5	2.5	79.4	82.2	3.5
8	129.2	146.7	13.5	413.9	437.3	5.7	69.3	69.9	0.9
9	114.1	134.8	18.1	377.6	367.1	2.8	53.9	61.0	13.2
10	107.6	124.1	15.3	340.5	306.0	10.1	56	54.8	2.1
Average			10.7			5.0			6.7

**Fig. 7** Predicted and measured three-axis cutting force waves, **a** No. 4 (CM). **b** No. 7 (CM). **c** No. 2 ( $P_0 = 250$  W). **d** No. 3 ( $P_0 = 500$  W). **e** No. 6 ( $P_0 = 500$  W). **f** No. 8 ( $P_0 = 500$  W)

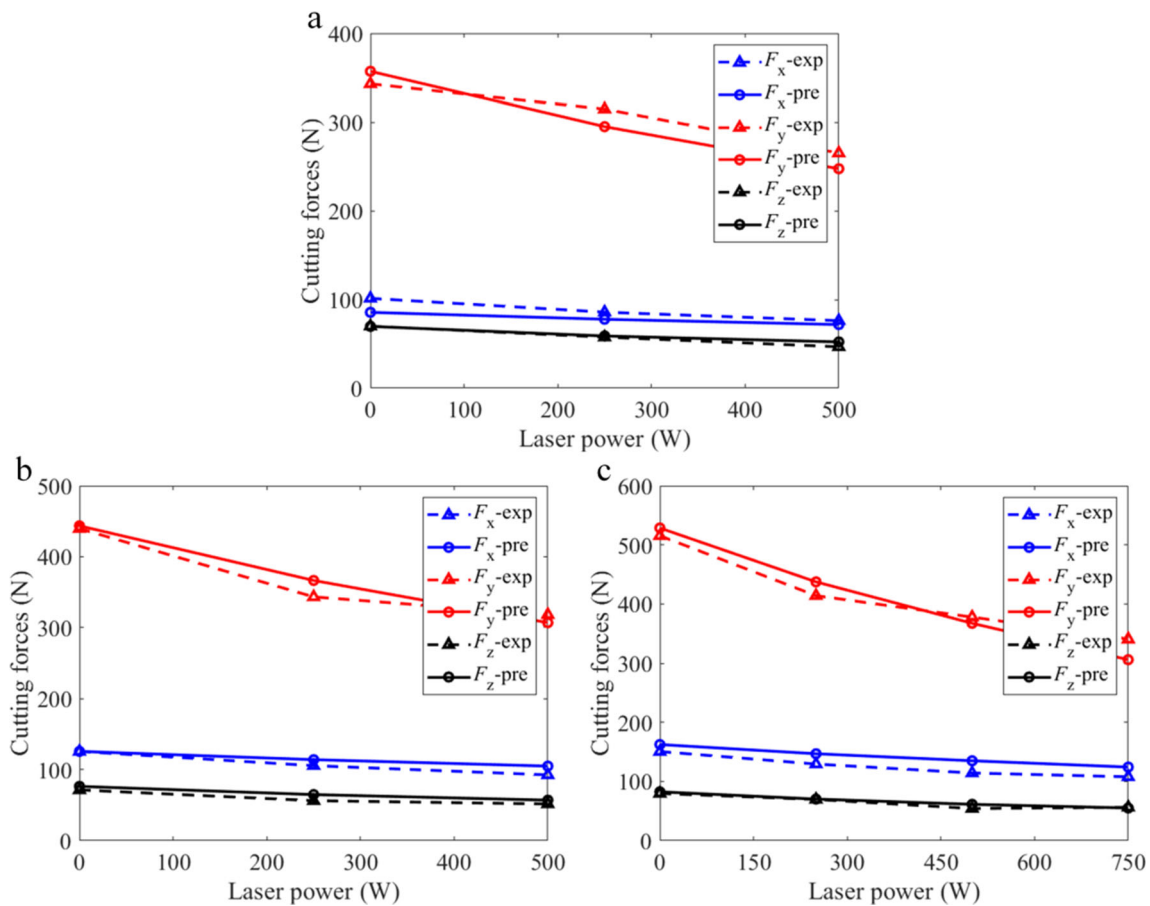


**Fig. 8** Variations of cutting forces amplitudes along laser power under different feed rates. **a**  $f_z = 0.05$  mm/tooth (Exp. Nos. 1–3). **b**  $f_z = 0.075$  mm/tooth (Exp. Nos. 4–6). **c**  $f_z = 0.1$  mm/tooth (Exp. Nos. 7–10)

and least sensitive to changes in laser scanning speed respectively.

By comparing Fig. 9a–c, it is found that, when the laser power is larger, the growth rate of the cutting force amplitude is smaller than that under a lower laser power condition, which indicates that the increase of the laser power can slow down the disadvantage caused by the faster laser scanning speed. The reason is that the increase of laser power can strengthen the material softening effect.

#### 4.3.3 Laser-tool distance (in the X direction)

Too small laser-tool distance will shorten the heating time, while too large laser-tool distance will prolong the cooling time after the material is heated, both of which will weaken the softening effect of the material. Figure 10 shows the effect of laser-tool distance in the X direction ( $d_1$ ) on the three-axis cutting force of LAM.  $d_1$  varied from 10 to 20 mm, and laser power  $P_0$  was 250 W and 500 W, respectively. Other process parameters were the same as experiment Nos. 1–3 in Table 2. As shown in the figure, the amplitude of the three-axis cutting force gradually increases with increasing laser-tool distance.

This is because the increase of laser-tool distance lengthens the cooling time before the material is cut, which weakens the softening effect and leads to a reduction in the preheating temperature of shear plane.

Figure 10a and b are drawn at a laser power of 250 W and 500 W respectively. It is not difficult to find that the amplitude of the three-axis cutting force in Fig. 10b changes more dramatically with the increase of laser-tool distance, which indicates that, the greater the laser power is, the more significant the influence of laser-tool distance on the three-axis cutting force will be.

## 5 Conclusions

In this paper, an analytical model is established to predict cutting forces in LAM. In the model, the effects of laser heating and plastic deformation on shear plane temperature and shear flow stress are considered simultaneously. And the proposed model is verified by LAM experiments. According to the experimental and predicted results, as well as the analyses reported above, the following conclusions can be drawn:

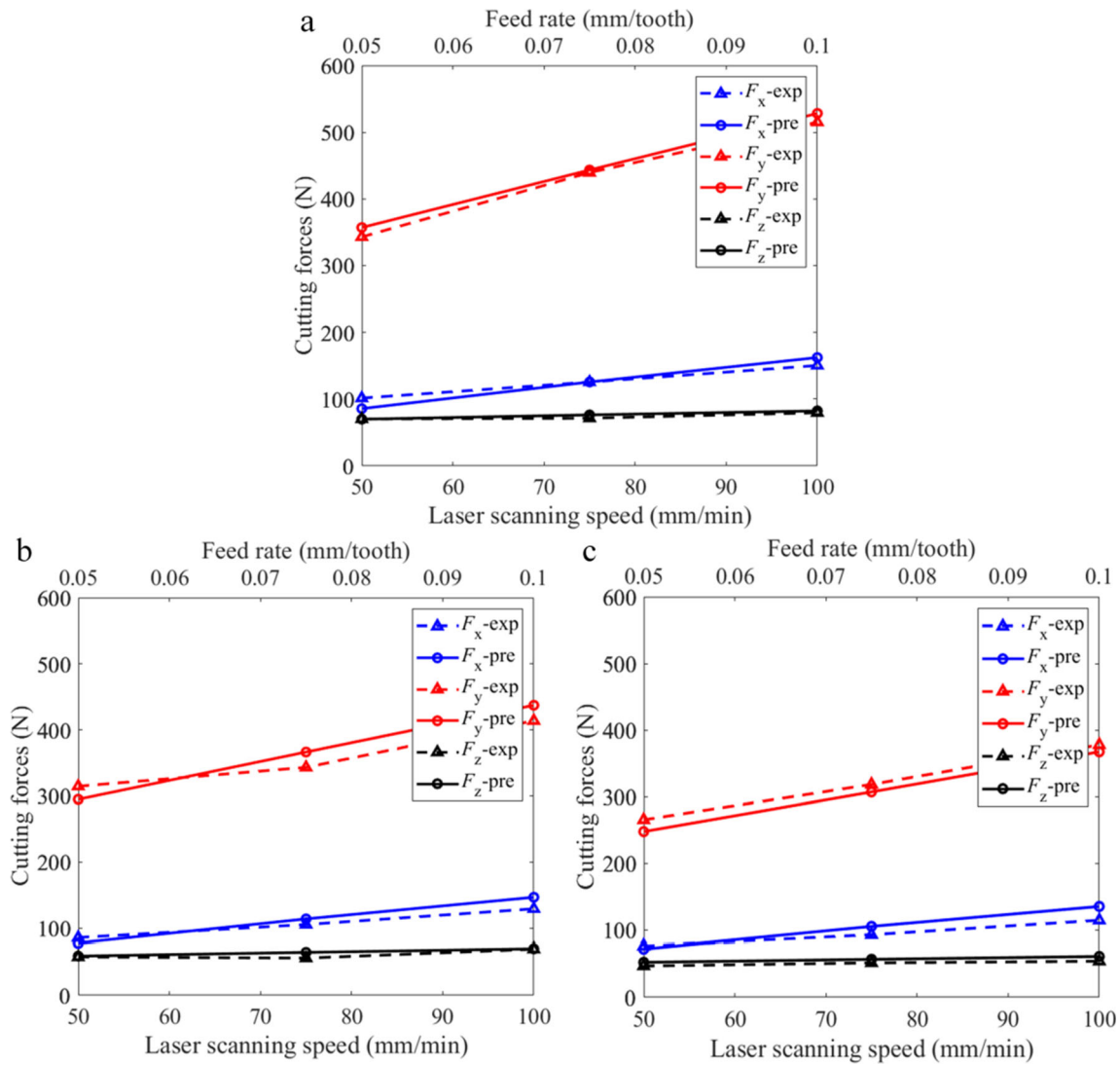


**Fig. 9** Variations of cutting force amplitudes along feed rate under different laser powers. **a**  $P_0 = 0$  (Exp. Nos. 1, 4, 7). **b**  $P_0 = 250$  W (Exp. Nos. 2, 5, 8). **c**  $P_0 = 500$  W (Exp. Nos. 3, 6, 9)

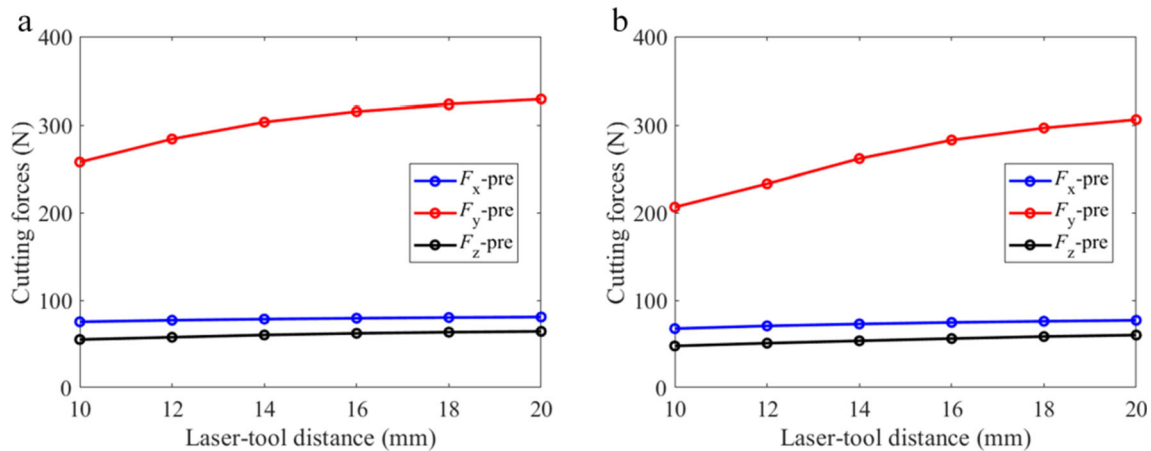


**Fig 10** Variations of cutting force amplitudes along laser-tool distance under different laser powers. **a**  $P_0 = 250$  W. **b**  $P_0 = 500$  W

- (1) The predicted results of cutting force agree well with measured data, which proves the feasibility of the model.
- (2) A method for solving the shear plane temperature and shear flow stress considering material softening effect of LAM is proposed. Compared with CM, higher shear plane temperature and lower shear flow stress are generated in LAM, which indicates that there is a significant material softening effect. This model can reflect the material flow behavior in LAM process better than the model established in Ref. [19].
- (3) The amplitude of the three-axis cutting force ( $F_x$ ,  $F_y$ ,  $F_z$ ) in LAM is reduced by up to 28.5%, 33.9%, and 29.5% respectively. The experimental results show that LAM of AerMet100 steel has a significant effect in reducing cutting forces.
- (4) Material softening effect is controlled by laser power, laser scanning speed, and laser-tool distance. The reduction of laser power, the acceleration of laser scanning speed, and the increase of laser-tool distance will weaken the degree of material softening, which reduces the preheating temperature of shear plane and increases shear flow stress, and finally leads to the increase of cutting force.

This work can be applied to optimize process parameters and reveal machining mechanism in LAM.

**Authors' contributions** Hang Zhang derived the formula of the article and write the code, and completed the model validation and the writing of the article. Haohao Zeng presented the article's preliminary idea, provided the experimental design, and mainly set up the experimental platform. Fangyu Peng and Rong Yan putted forward many constructive suggestions for the writing of the whole article. Wei Wang assisted in carrying out verification experiments.

**Funding** This work was supported by the National Natural Science Foundation of China under Grant No. 51775213, the National Natural Science Foundation of China under Grant No. 91860206, and the National Science Fund for Distinguished Young Scholars under Grant No. 51625502.

**Data availability** All data during the study and other related materials are available from the corresponding author by request.

## Compliance with ethical standards

**Competing interests** The authors declare that they have no conflict of interest.

**Ethical approval** Not applicable.

**Consent to participate** All authors and facilitators have certified their participation in this work.

**Consent to publish** All authors certify that they consent to publish the article. The article is the author's original work and has not been published in advance or considered for publication elsewhere.

## References

1. Chatterjee S, Mahapatra SS, Arora KS, Behera A (2020) Physical and mechanical characterization of dissimilar laser welded joints of AISI 316/Cu/SMA using fiber laser technology. *J Laser Appl* 32(3):032018. <https://doi.org/10.2351/7.0000003>
2. Chatterjee S, Sahoo SK, Swain B, Mahapatra SS, Roy T (2020) Quality characterization of dissimilar laser welded joints of Ti6Al4V with AISI 304 by using copper deposition technique. *Int J Adv Manuf Technol* 106(11):4577–4591. <https://doi.org/10.1007/s00170-020-04935-5>
3. Hu MF, Xie J, Su HH, Liu JN (2018) Study on laser-assisted dry micro-ground surface of difficult-to-cut materials. *Int J Adv Manuf Technol* 94(5-8):2919–2928. <https://doi.org/10.1007/s00170-017-1093-4>
4. Kim I-W, Lee C-M (2016) A study on the machining characteristics of specimens with spherical shape using laser-assisted machining. *Appl Therm Eng* 100:636–645. <https://doi.org/10.1016/j.applthermaleng.2016.02.005>
5. Anderson M, Patwa R, Shin YC (2006) Laser-assisted machining of Inconel 718 with an economic analysis. *Int J Mach Tools Manuf* 46(14):1879–1891. <https://doi.org/10.1016/j.ijmactools.2005.11.005>
6. Dandekar CR, Shin YC, Barnes J (2010) Machinability improvement of titanium alloy (Ti-6Al-4V) via LAM and hybrid machining. *Int J Mach Tools Manuf* 50(2):174–182. <https://doi.org/10.1016/j.ijmactools.2009.10.013>
7. Dumitrescu P, Koshy P, Stenekes J, Elbestawi MA (2006) High-power diode laser assisted hard turning of AISI D2 tool steel. *Int J Mach Tools Manuf* 46(15):2009–2016. <https://doi.org/10.1016/j.ijmactools.2006.01.005>
8. Venkatesan K (2017) The study on force, surface integrity, tool life and chip on laser assisted machining of Inconel 718 using Nd:YAG laser source. *J Adv Res* 8(4):407–423. <https://doi.org/10.1016/j.jare.2017.05.004>
9. Huang X, Zou F, Ming W, Xu J, Chen Y, Chen M (2020) Wear mechanisms and effects of monolithic Sialon ceramic tools in side milling of superalloy FGH96. *Ceram Int* 46(17):26813–26822. <https://doi.org/10.1016/j.ceramint.2020.07.157>
10. Chatterjee S, Mahapatra SS, Abhishek K (2016) Simulation and optimization of machining parameters in drilling of titanium alloys. *Simul Model Pract Theory* 62:31–48. <https://doi.org/10.1016/j.simpat.2015.12.004>
11. Liu C, Lei G, Jiang X, Xu W, Liu S, Yang T (2020) Analytical modeling of subsurface damage depth in machining of SiC<sub>p</sub>/Al composites. *Int J Mech Sci* 185:105874. <https://doi.org/10.1016/j.ijmecsci.2020.105874>
12. Ozel T, Pfefferkorn F (2007) Pulsed laser assisted micromilling for die/mold manufacturing. In: *Proceedings of the ASME International Conference on Manufacturing Science and Engineering*, pp 337–342
13. Xi Y, Birmingham M, Wang G, Dargusch M (2013) Finite element modeling of cutting force and chip formation during thermally assisted machining of Ti6Al4V alloy. *J Manuf Sci Eng Trans ASME* 135(6). <https://doi.org/10.1115/1.4025740>
14. Pan Z, Feng Y, Lu Y-T, Lin Y-F, Hung T-P, Hsu F-C, Lin C-F, Lu Y-C, Liang SY (2017) Microstructure-sensitive flow stress modeling for force prediction in laser assisted milling of Inconel 718. *Manuf Rev*:4. <https://doi.org/10.1051/mfreview/2017005>
15. Kim D-H, Lee C-M (2014) A study of cutting force and preheating-temperature prediction for laser-assisted milling of Inconel 718 and AISI 1045 steel. *Int J Heat Mass Transf* 71:264–274. <https://doi.org/10.1016/j.ijheatmasstransfer.2013.12.021>
16. Woo W-S, Lee C-M (2018) A study on the optimum machining conditions and energy efficiency of a laser-assisted fillet milling. *Int*

- J Precise Eng Manuf Green Technol 5(5):593–604. <https://doi.org/10.1007/s40684-018-0061-2>
17. Singh R, Melkote SN (2009) Force modeling in laser-assisted microgrooving including the effect of machine deflection. *J Manuf Sci Eng Trans ASME* 131(1). <https://doi.org/10.1115/1.3040076>
  18. Kumar M, Chang C-J, Melkote SN, Joseph VR (2013) Modeling and analysis of forces in laser assisted micro milling. *J Manuf Sci Eng Trans ASME* 135(4). <https://doi.org/10.1115/1.4024538>
  19. Elhami S, Razfar MR, Farahnakian M (2015) Analytical, numerical and experimental study of cutting force during thermally enhanced ultrasonic assisted milling of hardened AISI 4140. *Int J Mech Sci* 103:158–171. <https://doi.org/10.1016/j.ijmecsci.2015.09.007>
  20. Pan Z, Feng Y, Lu Y-T, Lin Y-F, Hung T-P, Hsu F-C, Liang SY (2017) Force modeling of Inconel 718 laser-assisted end milling under recrystallization effects. *Int J Adv Manuf Technol* 92(5-8): 2965–2974. <https://doi.org/10.1007/s00170-017-0379-x>
  21. Altintas Y (2012) *Manufacturing automation: metal cutting mechanics, machine tool vibrations, and CNC design*. Cambridge University Press, New York
  22. Waldorf DJ, DeVor RE, Kapoor SG (1998) A slip-line field for ploughing during orthogonal cutting. *J Manuf Sci Eng Trans ASME* 120(4):693–699. <https://doi.org/10.1115/1.2830208>
  23. Armarego E, Brown RH (1969) *The machining of metals*. Prentice Hall, New York
  24. Stabler G (1951) The fundamental geometry of cutting tools. *Proc Inst Mech Eng* 165(1):14–26
  25. Manjunathaiah J, Endres WJ (2000) A new model and analysis of orthogonal machining with an edge-radiused tool. *J Manuf Sci Eng Trans ASME* 122(3):384–390. <https://doi.org/10.1115/1.1285886>
  26. Manjunathaiah J (1998) *Analysis and a new model for the orthogonal machining process in the presence of edge-radiused (non-sharp) tools*. dissertation, The University of Michigan, Ann Arbor
  27. Basuray P, Misra B, Lal G (1977) Transition from ploughing to cutting during machining with blunt tools. *Wear* 43(3):341–349
  28. Ozlu E, Budak E, Molinari A (2009) Analytical and experimental investigation of rake contact and friction behavior in metal cutting. *Int J Mach Tools Manuf* 49(11):865–875. <https://doi.org/10.1016/j.ijmactools.2009.05.005>
  29. Merchant ME (1945) Mechanics of the metal cutting process. II. Plasticity conditions in orthogonal cutting. *J Appl Phys* 16(6):318–324
  30. Zeng H, Yan R, Wang W, Zhang H, Yan J, Peng F (2020) Analytical modeling of the heat-affected zone in laser-assisted milling of AerMet100 steel. *Int J Adv Manuf Technol* 109:2481–2490. <https://doi.org/10.1007/s00170-020-05821-w>
  31. Yan R, Zeng HH, Peng FY, Yang S, Dong Q, Zhou L (2015) Analytical modeling and experimental validation of workpiece temperature variation in bull-nose end milling. *Int J Adv Manuf Technol* 86(1-4):155–168. <https://doi.org/10.1007/s00170-015-8130-y>
  32. Srinivasa YV, Shunmugam MS (2013) Mechanistic model for prediction of cutting forces in micro end-milling and experimental comparison. *Int J Mach Tools Manuf* 67:18–27. <https://doi.org/10.1016/j.ijmactools.2012.12.004>
  33. Tounsi N, Vincenti J, Otho A, Elbestawi MA (2002) From the basic mechanics of orthogonal metal cutting toward the identification of the constitutive equation. *Int J Mach Tools Manuf* 42(12):1373–1383. [https://doi.org/10.1016/s0890-6955\(02\)00046-9](https://doi.org/10.1016/s0890-6955(02)00046-9)
  34. Zeng H, Yan R, Du P, Zhang M, Peng F (2018) Notch wear prediction model in high speed milling of AerMet100 steel with bull-nose tool considering the influence of stress concentration. *Wear* 408–409:228–237. <https://doi.org/10.1016/j.wear.2018.05.024>

**Publisher's note** Springer Nature remains neutral with regard to jurisdictional claims in published maps and institutional affiliations.